A Signal Temporal Logic Motion Planner for Bird Diverter Installation Tasks with Multi-Robot Aerial Systems

Alvaro Caballero[1†] and Giuseppe Silano[2*†]

[1]Department of System Engineering and Automation, University of Seville, Camino de los Descubrimientos s/n, Seville, 41092, Spain.

[2*]Department of Generation Technologies and Materials, Ricerca sul Sistema Energetico (RSE) S.p.A., Via Rubattino 54, Milan, 20134, Italy and Department of Cybernetics, Czech Technical University in Prague, Karlovo Namesti 13, Prague, 12135, Czech Republic.

*Corresponding author(s). E-mail(s): giuseppe.silano@fel.cvut.cz;
Contributing authors: alvarocaballero@us.es;
†These authors contributed equally to this work.

Abstract

This paper investigates the problem of task assignment and trajectory generation for the installation of bird diverters with a fleet of multirotors leveraging on Signal Temporal Logic (STL) specifications. We extend our previous motion planner to compute feasible and constrained trajectories, taking into account payload capacity limitations and recharging constraints. The proposed planner ensures the continuity of the operation, while guaranteeing compliance with safety requirements and mission fulfillment. Additionally, an event-based replanning strategy is proposed to react to unforeseen failures. An energy minimization term is also considered to implicitly save multirotor flight time during installation operations. Numerical simulations in MATLAB, Gazebo, and field experiments demonstrate the performance of the approach and its validity in mock-up scenarios.

Keywords: Multi-Robot Systems, Aerial Systems: Applications, Task and Motion Planning, Optimization and Optimal Control

1 Introduction

Power lines are among the most important civil infrastructure in any country. Over thousands of kilometers, they supply energy to millions of people. In order to minimize power outages and improve network reliability, electricity supply companies invest considerable resources in inspection and maintenance operations. Given the high risk of bird collisions [1], a key activity is the installation of bird diverters on top of power lines (see Figure 1) in order to increase their visibility [2]. This task is typically carried out by manned helicopters and experienced crews with the following associated drawbacks: (i) it is a time-consuming task, as power lines are usually at locations of difficult access; and (ii) it is dangerous, as installation is performed at height on active lines.

Unmanned Aerial Vehicles (UAVs) are a promising solution to automate this task [3, 4], as they can support continuous operation covering long-range distances. Furthermore, they can be equipped with lightweight manipulation devices to support installation operations autonomously [3, 5–7]. Due to their limited battery and payload capacity, the use of a team with multiple UAVs is of great interest as it could speed up the process and cover large-scale scenarios. However, this problem is challenging from a planning

Figure 1: An example of bird diverters installed on a medium voltage power line infrastructure.

perspective; operations to recharge batteries or diverters need to be scheduled, safe trajectories without collisions are needed, vehicle dynamics and energy consumption models should be considered, among other concerns.

Therefore, advanced task and motion planning techniques are needed to enable the installation of bird diverters with multi-UAV teams, meeting critical safety requirements while ensuring compliance of the mission objectives. Temporal Logic (TL) can serve this purpose by providing a mathematical framework for expressing complex specifications, which combine natural language commands with temporal and Boolean operators [8]. In particular, Signal Temporal Logic (STL) [9] is endowed with a metric called *robustness*, which allows one to not only to assess whether the system execution meets the requirements, but also to provide a measure of how well these requirements have been met. This results in an optimization problem aimed at maximizing this robustness score, providing the best feasible trajectory for the system while meeting the desired specifications.

This paper proposes a multi-UAV motion planner leveraging on STL specifications for installing bird diverters in power lines. The mission requirements are encoded as an STL formula, whose robustness is maximized by setting up a nonlinear non-convex *max-min* optimization problem. In order to tackle the complexity of this nonlinear optimization, a hierarchical approach is implemented, first solving a Mixed-Integer Linear Programming (MILP) problem and then feeding the final STL optimizer.

1.1 Related work

This paper addresses a complex multi-UAV motion problem, where compliance with vehicle dynamics, collision avoidance, limited mission time, and payload capacity must be taken into account. Sampling-based planners [10], such as the well-known Rapidly-exploring Random Tree (RRT) and its multiple variants, can compute collision-free trajectories in high-dimensional configuration spaces in reasonable time. There are also extensions that minimize energy consumption and deal with vehicle dynamics constraints [11, 12], although convergence has not been proven. However, RRT-based methods do not natively cope with payload capacity restrictions and face difficulties addressing complex nonlinear problems or multi-robot settings. In order to achieve real-time performance, motion primitives have also been explored for UAV optimal trajectory planning [13, 14].

In case the application requires visiting several locations to complete the mission, optimization approaches based on the Vehicle Routing Problem (VRP) formulation have been proposed [15]. Since VRP variants are NP-hard combinatorial problems, many works sacrifice optimality by proposing heuristic approaches [16]. Although these methods can address UAV capacity and mission time constraints, they struggle to deal with obstacle avoidance and multi-vehicle dynamics [17]. Hierarchical approaches [18, 19] leveraging on Probabilistic Roadmaps (PRMs) and kinodynamic Stable Sparse RRT (SST) methods have been investigated to generate collision-free and minimum-time flight trajectories. However, the problems discussed do not consider either the UAV payload capacity or the multi-UAV settings.

Alternatively, thanks to the increase in computational resources on board UAVs and the recent advances in efficient numerical methods, receding horizon approaches for optimal control are flourishing to tackle multi-UAV trajectory planning [20]. Centralized methods for non-convex optimization [21] have been proposed along with distributed Model Predictive Control (MPC)-based algorithms [22, 23]. Although these types of methods can efficiently compute safe and optimal trajectories for multiple UAVs in the problem formulation, they do not take into account high-level mission specifications (such as time interval or ordering constraints), nor task planning in problem formulation.

Additionally, there are publications in the literature that enhance motion planning for multi-robot systems using formal specification languages [8, 9]. The authors in [24] propose the extraction of local specifications that are assigned to particular robots to deal with multi-robot trajectory planning. The motion capabilities of each robot are represented using a transition system, whose modeling may become computationally expensive with an increase in the number of agents and tasks. On the contrary, Control Barrier Functions (CBFs) [25] have been shown as suitable for efficiently solve motion planning problems. However, they can only be applied to a fragment of the STL formula, restricting their application to simple scenarios [26]. In [27], the authors present robust algorithms for multi-robot coordination that encode high-level TL specifications into an MILP problem. However, their sequential multi-robot RRT algorithm leads to suboptimal trajectories. A reinforcement learning approach for multi-agent systems has been presented in [28]. The authors focus on finite abstractions and deterministic systems. However, such an approach requires methodological advances, as it still poses computational challenges for complex STL formulae.

1.2 Contributions

This paper proposes a novel task and motion planning approach for installing bird diverters on power lines with a team of multirotors. The method leverages STL to generate optimal trajectories that are dynamically feasible (i.e., that comply with vehicle dynamics and velocity and acceleration limits) and fulfill several mission specifications: collision avoidance between UAVs and the environment, bounded UAV payload capacities, and reaching all target regions within the total given mission time while remaining long enough for diverter installation. This results in a complex nonlinear optimization problem that we tackle by means of a novel hierarchical approach. The so-formulated problem extends our previous work [29] by addressing the installation of bird diverters, which implies computing dynamically feasible trajectories that take into account payload capacity limitations, as well as refilling stations for long-endurance operation. Moreover, a novel procedure to compute the initial guess solution for the optimization problem is proposed. The main contributions of this paper are as follows:

- The multi-UAV planning problem for installing diverters on power lines is formulated in Section 2. Given that, STL specifications are extracted (see Section 3) and used to set up an optimization problem that integrates task and motion planning, providing dynamically feasible trajectories complying with safety requirements (i.e., obstacle avoidance and mutual safety distances) and mission fulfillment.
- The proposed STL optimization problem (Section 4) yields global optimal solutions, but its nonlinear non-convex *max-min* nature makes it difficult to solve. These types of problems are tackled by dynamic programming approaches, which are known to suffer from their dependence on the initial guess [30]. As a result, we propose a hierarchical approach where this initial guess is generated by an MILP approach (Section 4.2), which works on a simplified set of constraints of the original problem, neglecting obstacle avoidance, safety requirements, vehicle dynamics, and time mission specifications. The sequence of target regions to install diverters per UAV is output, as well as their corresponding refilling operations to load additional diverters. Then, motion primitives are used to approximate UAV dynamics and generate feasible trajectories (position, velocity, and acceleration) connecting each pair of points. Finally, these trajectories are used as the initial guess for the global STL planner, which helps its convergence towards solutions that meet all requirements.
- An event-based replanning strategy (Section 4.3) is proposed to react to unforeseen UAV failures, making the method valid for scenarios with dynamic conditions. Moreover, an extension to come up with an energy-aware planner (Section 4.4) is included. This new version of the planner includes an energy minimization term to implicitly extend the endurance of the multirotors during the mission.
- Numerical simulations in MATLAB (Sections 5) evaluate the overall performance of the method in terms of the fulfillment of mission specifications and the effectiveness of including the novel initialization procedure to address the STL optimization. Furthermore, Gazebo simulations and field experiments (Section 5.4) in a mock-up setting showcase its validity and feasibility for real scenarios. Conclusions and related future extensions are discussed in Section 6.

2 Problem Description

This paper addresses the problem of installing bird diverters on power lines with a team of δ UAVs, denoting $\mathcal{D}$ as the set of UAVs. Figure 2 depicts a scheme of the scenario. The goal is to visit a sequence of predefined *target regions* for installation distributed across the upper cables that hold between consecutive towers [4]. Each region represents a potential 3D space where a diverter could be installed. Defining regions

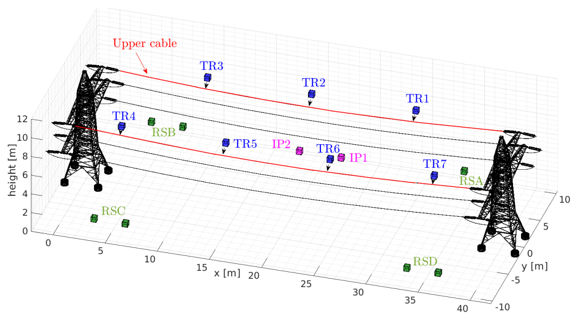

Figure 2: Example scenario for the installation of bird diverters. Target regions (TR) are represented in blue, while UAVs' initial position (IP) and refilling stations (RS) are depicted in magenta and green, respectively. A red line denotes the upper cables between the power towers.

instead of point locations helps simplify the problem. Once the UAV reaches a region, it is assumed that an onboard low-level controller takes care of the installation operation [3, 6]. UAVs are assumed to be multirotors with limited velocity, acceleration, and payload capacity. That is to say, the number of diverters that can be carried on board is bounded. These payload capacities can be heterogeneous for each UAV, while dynamic constraints are homogeneous (velocity and acceleration bounds). Additionally, a set of refilling stations are scattered on the ground along the power line. These stations are safe places where the multirotors can (within a bounded and known time interval) load new diverters to get back into operation. Given the velocity and acceleration limitations of the vehicles, and assuming a bounded operation time for each diverter installation, the battery constraints can be translated into a maximum traveled distance for each UAV. This is equivalent to constraining their mission time, under the assumption that UAVs have comparable flight times. The objective is to plan trajectories for the multirotors to accomplish the mission in the specified maximum time, while complying with the aforementioned dynamics and capacity constraints, as well as safety requirements, i.e., avoiding obstacles in the scenario and maintaining a safety distance between UAVs. A map of the environment with a polyhedral representation of the obstacles (e.g., power towers and cables) is assumed as known in advance.

3 Preliminaries

Let us consider a discrete-time dynamical system $x_{k+1} = f(x_k, u_k)$, where $x_{k+1}, x_k \in \mathcal{X} \in \mathbb{R}^n$ represent the next and current states of the system, respectively, and $u_k \in \mathcal{U} \in \mathbb{R}^m$ is the control input. Let us also assume that $f\colon \mathcal{X} \times \mathcal{U} \to \mathcal{X}$ is differentiable in both arguments. Therefore, given an initial state $x_0 \in \mathcal{X}_0 \in \mathbb{R}^n$ and a time vector $\mathbf{t} = (t_0, \dots, t_N)^\top \in \mathbb{R}^{N+1}$, with $N \in \mathbb{N}_{>0}$ being the number of samples that describe the evolution of the system with the sampling period $T_s \in \mathbb{R}_{>0}$, we can define the finite control input sequence $\mathbf{u} = (u_0, \dots, u_{N-1})^\top \in \mathbb{R}^N$ as the input to provide the system to obtain the unique sequence of states $\mathbf{x} = (x_0, \dots, x_N)^\top \in \mathbb{R}^{N+1}$.

Hence, we can define the state sequence $\mathbf{x}$ and the control input sequence $\mathbf{u}$ of a multirotor as $\mathbf{x} = (\mathbf{p}^{(1)}, \mathbf{v}^{(1)}, \mathbf{p}^{(2)}, \mathbf{v}^{(2)}, \mathbf{p}^{(3)}, \mathbf{v}^{(3)})^\top$ and $\mathbf{u} = (\mathbf{a}^{(1)}, \mathbf{a}^{(2)}, \mathbf{a}^{(3)})^\top$, where $\mathbf{p}^{(j)}$, $\mathbf{v}^{(j)}$, and $\mathbf{a}^{(j)}$, with $j = \{1, 2, 3\}$, represent the sequences of position, velocity, and acceleration of the vehicle along the j axis of the inertial frame, respectively. We denote with $p_k^{(j)}$, $v_k^{(j)}$, $a_k^{(j)}$ and t_k, with $k \in \mathbb{N}_{\geq 0}$, the k-th elements of the vectors $\mathbf{p}^{(j)}$, $\mathbf{v}^{(j)}$, $\mathbf{a}^{(j)}$, and $\mathbf{t}$, respectively.

3.1 Signal temporal logic

Definition 1 *(Signal Temporal Logic)*: STL was introduced for the first time in [9] to monitor the behavior of real-valued signals. Such a logic allows the description of complex system behaviors in a succinct and unambiguous way, encoding requirements and specifications into a single formula φ [9]. For example, "at least two vehicles need to survey regions A and B, one needs to visit region C within the time interval $[t_1, t_2]$, while all must comply with safety requirements". The full description of the STL syntax and semantics can be found in [9, 31] and is not given here for the sake of brevity. In short, an STL formula φ is defined on a set of predicates, i.e., atomic prepositions that yield simple operations, such as belonging to a region or comparisons of real values. These predicates are combined using Boolean ($\neg$, $\wedge$, $\vee$) and temporal ($\Diamond$, $\Box$, $\mathcal{U}$) operators. The resulting STL formula φ is considered valid if the expression takes a true ($\top$) logic value, and invalid ($\bot$) otherwise. For instance, informally, $\varphi_1 \mathcal{U}_I \varphi_2$ means that the predicate φ_2 must hold at some point in the time interval I and, until then, φ_1 must hold without interruption.

3.2 Robust signal temporal logic

Definition 2 *(STL Robustness)*: The presence of system uncertainties, a dynamic environment, and unforeseen events can affect the satisfaction of an STL formula φ. In an attempt to have a maneuverability margin of satisfaction of φ, measuring how well (poorly) a given specification is met, the concept of *robust semantic* for STL formulae has been formulated [9, 31, 32]. This *robustness*, denoted as ρ, is a quantitative metric that guides the optimization problem derived towards the best feasible solution to achieve mission satisfaction. This value can be formally described by using the following formulae in a recursive manner:

$$\begin{aligned}
\rho_{\neg\varphi}(\mathbf{x}, t_k) &= -\rho_{\varphi}(\mathbf{x}, t_k), \\
\rho_{\varphi_1 \wedge \varphi_2}(\mathbf{x}, t_k) &= \min\left(\rho_{\varphi_1}(\mathbf{x}, t_k), \rho_{\varphi_2}(\mathbf{x}, t_k)\right), \\
\rho_{\varphi_1 \vee \varphi_2}(\mathbf{x}, t_k) &= \max\left(\rho_{\varphi_1}(\mathbf{x}, t_k), \rho_{\varphi_2}(\mathbf{x}, t_k)\right), \\
\rho_{\Box_I \varphi}(\mathbf{x}, t_k) &= \min_{t'_k \in [t_k + I]} \rho_{\varphi}(\mathbf{x}, t'_k), \\
\rho_{\Diamond_I \varphi}(\mathbf{x}, t_k) &= \max_{t'_k \in [t_k + I]} \rho_{\varphi}(\mathbf{x}, t'_k), \\
\rho_{\varphi_1 \mathcal{U} \varphi_2}(\mathbf{x}, t_k) &= \max_{t'_k \in [t_k + I]} \Big(\min\left(\rho_{\varphi_2}(\mathbf{x}, t'_k)\right), \\
&\qquad \min_{t''_k \in [t_k, t'_k]} \left(\rho_{\varphi_1}(\mathbf{x}, t''_k)\right) \Big),
\end{aligned}$$

where $t_k + I$ is meant herein as the Minkowski sum between the scalar t_k and the time interval I. The above formulae are composed of a set of *predicates*, each resulting as true if its robustness value is greater than or equal to zero, and false otherwise. The whole formula works as a logic formula, where it is false if at least one predicate is false. For the case of study, one example could be being inside a target region or being outside an obstacle region, with regions described by a certain number of predicates. Further details can be found in [8, 9, 31]. In this case, we say that $\mathbf{x}$ satisfies the STL formula φ at time t_k if $\rho_{\varphi}(\mathbf{x}, t_k) > 0$, and $\mathbf{x}$ violates φ if $\rho_{\varphi}(\mathbf{x}, t_k) \leq 0$.

Thus, we can compute the control inputs $\mathbf{u}$ that maximize the robustness over the set of finite state and input sequences $\mathbf{x}$ and $\mathbf{u}$, respectively. This optimal sequence $\mathbf{u}^{\star}$ is valid if $\rho_{\varphi}(\mathbf{x}^{\star}, t_k)$ is positive, where $\mathbf{x}^{\star}$ and $\mathbf{u}^{\star}$ obey the dynamical system. The larger $\rho_{\varphi}(\mathbf{x}^{\star}, t_k)$ is, then the more robust the behavior of the system.

Definition 3 *(Smooth Approximation)* [26]: Let us consider $\lambda \in \mathbb{R}_{>0}$ as a tunable parameter. The smooth approximation of the $\min$ and $\max$ operators with β-predicate arguments is

$$\begin{aligned}
\max(\rho_{\varphi_1}, \dots, \rho_{\varphi_\beta}) &\approx \frac{\sum_{i=1}^{\beta} \rho_{\varphi_i} e^{\lambda \rho_{\varphi_i}}}{\sum_{i=1}^{\beta} e^{\lambda \rho_{\varphi_i}}}, \\
\min(\rho_{\varphi_1}, \dots, \rho_{\varphi_\beta}) &\approx -\frac{1}{\lambda} \log \left(\sum_{i=1}^{\beta} e^{-\lambda \rho_{\varphi_i}} \right).
\end{aligned}$$

This approximation is asymptotically complete and smooth everywhere, as the widely known Log-Sum-Exponential (LSE) approximation [31] in our previous work [29]. It is also sound, as it does not over approximate the $\max$ operator. In short, *asymptotical completeness* means that the approximation of the final robustness formula $\tilde{\rho}_{\varphi}(\mathbf{x})$ can be arbitrarily close to the true robustness $\rho_{\varphi}(\mathbf{x})$ with $\lambda \to \infty$. *Smooth everywhere* ensures that the approximation is infinitely differentiable, so gradient-based optimization algorithms can be used to find a solution to the problem. *Soundness* implies that an optimal sequence $\mathbf{u}^{\star}$ with strictly positive robustness ($\rho_{\varphi}(\mathbf{x}) > 0$) satisfies the specification φ, and an optimal sequence $\mathbf{u}^{\star}$ with strictly negative robustness ($\rho_{\varphi}(\mathbf{x}) < 0$) violates it. The larger λ, then the closer the approximation of the true robustness (Def. 2).

Definition 4 *(STL Motion Planner)* [29]: Starting from mission specifications encoded as STL formula φ, and replacing its robustness $\rho_{\varphi}(\mathbf{x})$ with the smooth approximation[1] $\tilde{\rho}_{\varphi}(\mathbf{x})$ (Def. 3), the generation of multirotor trajectories can be formulated as the optimization problem

$$\begin{aligned}
\underset{\mathbf{p}^{(j)}, \mathbf{v}^{(j)}, \mathbf{a}^{(j)}}{\text{maximize}} \quad & \tilde{\rho}_{\varphi}(\mathbf{p}^{(j)}, \mathbf{v}^{(j)}) \\
\text{s.t.} \quad & |v_k^{(j)}| \leq \bar{v}^{(j)}, |a_k^{(j)}| \leq \bar{a}^{(j)}, \\
& \mathbf{S}^{(j)}, \forall k = \{0, 1, \dots, N-1\},
\end{aligned} \qquad (1)$$

where $\bar{v}^{(j)}$ and $\bar{a}^{(j)}$ are the maximum values desired in the velocity and acceleration module along the motion, respectively, and $\mathbf{S}^{(j)}(p_k^{(j)}, v_k^{(j)}, a_k^{(j)}) = (p_{k+1}^{(j)}, v_{k+1}^{(j)}, a_{k+1}^{(j)})^{\top}$ are multirotor motion primitives along each j axis encoding the splines presented in [29, eq. (2)]. Note, that for the simplicity of notation as described in [29], the optimization problem (1) is expressed for a single multirotor where the velocity

[1] ρ_{φ} uses non-differentiable functions $\min$ and $\max$. A good approach to mitigating computational complexity is to adopt a smooth approximation $\tilde{\rho}_{\varphi}$ of the robustness function ρ_{φ}.

and acceleration limits are considered to be symmetric along the axes of the inertial frame.

4 Problem Solution

In this section, the STL framework presented in Section 3 is used to formulate the optimization problem in Section 2. This yields a nonlinear non-convex max-min problem formulated as a Nonlinear Programming (NLP) formulation solved by dynamic programming (Section 4.1). Finding a solution for this type of nonlinear problem in a reasonable time is difficult, as solvers easily get stuck in local optima [30, 33]. This issue is circumvented by generating an initial guess from a simplified MILP formulation without considering obstacle avoidance, safety requirements, vehicle dynamics, and time mission specifications (Section 4.2), which eases the search for a global solution. The proposed framework incorporates a mechanism for mission replanning in order to account for UAV failures (Section 4.3). Finally, the original motion planner is improved with an additional optimization term to minimize energy consumption (Section 4.4).

4.1 STL motion planner

In this section, the mission specifications for the problem in Section 2 are extracted to obtain the corresponding STL formula, φ. Missions to install bird diverters have two types of specifications. First, the safety requirements must be fulfilled throughout the whole operation time t_N; UAVs have to stay within the workspace (φ_{ws}), while avoiding collisions with obstacles around (φ_{obs}) and keeping safety distances with other UAVs (φ_{dis}). Second, task requirements need to be satisfied at specific time intervals throughout the mission; all target regions must be visited once by a UAV, which remains there for an installation time t_{ins} (φ_{tr}). Given their limited payload capacity, UAVs should visit a refilling station and stay there for a refilling time t_{rs} once they run out of onboard diverters, to be supplied with more (φ_{cap}). Lastly, each UAV should fly to its closest refilling station after completing its installation operations (φ_{rs}). All mission specifications can be encoded in the STL formula

$$\varphi = \Box_{t_N} \varphi_{\text{ws}} \wedge \varphi_{\text{obs}} \wedge \varphi_{\text{dis}} \bigwedge \Diamond_{t_N} (\varphi_{\text{tr}} \wedge \varphi_{\text{cap}}) \,\mathcal{U} \varphi_{\text{rs}}, \quad (2)$$

with

$$\varphi_{\text{ws}} = \mathbf{p}^{(j)} \in (\underline{p}^{(j)}_{\text{ws}}, \bar{p}^{(j)}_{\text{ws}}), \quad (3a)$$

$$\varphi_{\text{obs}} = \forall_{\text{obs}}\, \mathbf{p}^{(j)} \notin (\underline{p}^{(j)}_{\text{obs}}, \bar{p}^{(j)}_{\text{obs}}), \quad (3b)$$

$$\varphi_{\text{dis}} = \forall_{\{n,m\}\in\mathcal{D},\, n\neq m} \|{}^{n}\mathbf{p} - {}^{m}\mathbf{p}\| > \Gamma, \quad (3c)$$

$$\varphi_{\text{tr}} = \forall_{\text{tr}}\, \Box_{t_{\text{ins}}} \mathbf{p}^{(j)} \in (\underline{p}^{(j)}_{\text{tr}}, \bar{p}^{(j)}_{\text{tr}}), \quad (3d)$$

$$\varphi_{\text{cap}} = \Box_{t_{\text{rs}}} (c == 0)\, \mathbf{p}^{(j)} \in (\underline{p}^{(j)}_{\text{rs}}, \bar{p}^{(j)}_{\text{rs}}), \quad (3e)$$

$$\varphi_{\text{rs}} = \mathbf{p}^{(j)} \in (\underline{p}^{(j)}_{\text{rs}}, \bar{p}^{(j)}_{\text{rs}}), \quad (3f)$$

where (3a) imposes the multirotor position $\mathbf{p}^{(j)}$ to stay within the boundaries of the workspace area, with $\underline{p}^{(j)}_{\text{ws}}$ and $\bar{p}^{(j)}_{\text{ws}}$ denoting its minimum and maximum values along the j axis of the inertial frame. Similarly, (3b), (3d), (3e), and (3f) set the obstacle avoidance, diverter installation, payload capacity, and mission completion specifications, respectively, where $c \in \mathbb{N}_{>0}$ represents the payload capacity of the multirotor (i.e., the number of loaded diverters) and $\underline{p}^{(j)}_{\text{obs}}$, $\underline{p}^{(j)}_{\text{tr}}$, $\underline{p}^{(j)}_{\text{rs}}$, $\bar{p}^{(j)}_{\text{obs}}$, $\bar{p}^{(j)}_{\text{tr}}$ and $\bar{p}^{(j)}_{\text{rs}}$ are the vertices of rectangular regions[2] along the j axis of the inertial frame used to identify obstacles, target regions, and refilling stations, respectively. Finally, (3c) is the safety distance requirement running over all UAVs, with $\Gamma \in \mathbb{R}_{>0}$ being a threshold value and $\{n,m\} \in \mathcal{D}$ the UAV indices. Note that in order to make this paper more readable, in (2) we simplified the notation by providing the STL formula φ for a single multirotor. However, with an appropriate set of summations and indices, it is not complicated to extend the formula φ to include all UAVs in the team. Actually, the STL optimization (1) for tackling the bird diverter installation problem is formulated by considering the team of multirotors and, hence, all the necessary sequences of state variables $\mathbf{x}$ and control inputs $\mathbf{u}$ to describe the multirotors' trajectories.

Using the specifications in (2), the optimization problem in Def. 4 is set up to compute feasible trajectories that achieve the maximum smooth robustness $\tilde{\rho}_{\varphi}(\mathbf{x})$ with respect to those mission specifications φ. To this end, the robustness score of each predicate needs to be computed. In the STL formula (2), there are two types of predicates: those evaluating whether the UAV position does or does not belong

[2]Similarly to $\underline{p}^{(j)}_{\text{ws}}$ and $\bar{p}^{(j)}_{\text{ws}}$, with $\underline{p}^{(j)}_{\text{obs}}$, $\underline{p}^{(j)}_{\text{tr}}$ and $\underline{p}^{(j)}_{\text{rs}}$, and with $\bar{p}^{(j)}_{\text{obs}}$, $\bar{p}^{(j)}_{\text{tr}}$ and $\bar{p}^{(j)}_{\text{rs}}$, we denote the minimum and maximum values of obstacles, target regions, and refilling stations along the j axis of the inertial frame, respectively.

to a specific region, (3a), (3b), (3d), (3e), and (3f), and the safety requirement (3c), evaluating the distance between UAVs. Robustness values are measured in terms of Euclidean distance. In predicates from the first group, a UAV that lies within the region has a positive robustness, and the greater the minimum Euclidean distance to the region's boundaries along the trajectory, the larger that robustness. There is an inversion in (3b), where belonging to the obstacle region means a negative robustness. In the safety distance predicate (3c), the robustness is positive when the distance between UAVs is greater than the threshold Γ. The larger the minimum Euclidean distance between UAVs along the trajectory, the higher the robustness. More formally, for the predicates of the first type, taking the φ_{ws} predicate (3a) as an example, we can write

$$\rho_{\varphi_{\text{ws}}} = \min_k \left(\min(\rho_{\bar{\varphi}^{(1)}}, \rho_{\underline{\varphi}^{(1)}}, \rho_{\bar{\varphi}^{(2)}}, \rho_{\underline{\varphi}^{(2)}}, \rho_{\bar{\varphi}^{(3)}}, \rho_{\underline{\varphi}^{(3)}}) \right), \quad (4)$$

with

$$\rho_{\bar{\varphi}^{(j)}} = \bar{p}^{(j)}_{\text{ws}} - p^{(j)}_k, \quad \rho_{\underline{\varphi}^{(j)}} = p^{(j)}_k - \underline{p}^{(j)}_{\text{ws}}.$$

In an equivalent way, the robustness score of the non-belonging predicate φ_{obs} (3b) can be computed by inverting each minimum distance for each sample along the trajectory. Namely, we can write

$$\rho_{\varphi_{\text{obs}}} = \min_k \left(-\min(\rho_{\bar{\varphi}^{(1)}}, \rho_{\underline{\varphi}^{(1)}}, \rho_{\bar{\varphi}^{(2)}}, \rho_{\underline{\varphi}^{(2)}}, \rho_{\bar{\varphi}^{(3)}}, \rho_{\underline{\varphi}^{(3)}}) \right), \quad (5)$$

where $\rho_{\bar{\varphi}^{(j)}}$ and $\rho_{\underline{\varphi}^{(j)}}$, with $j = \{1, 2, 3\}$, can be computed by replacing $\bar{p}^{(j)}_{\text{ws}}$ and $\underline{p}^{(j)}_{\text{ws}}$ in (4) with $\bar{p}^{(j)}_{\text{obs}}$ and $\underline{p}^{(j)}_{\text{obs}}$, respectively. On the contrary, the robustness score of the safety requirement predicate φ_{dis} (3c) can be expressed as

$$\rho_{\varphi_{\text{dis}}} = \min_k \left(\min_{\forall \{n,m\} \in \mathcal{D},\, n \neq m} (\|{}^n p_k - {}^m p_k\| - \Gamma) \right), \quad (6)$$

where the minimum distance between UAVs is computed for each time step (t_k) in the trajectory, and then the $\min$ value of that vector of minimum distances.

It should be noted that the coupled nature of mission requirements makes it necessary to plan all UAV trajectories in a joint optimization problem. Furthermore, the so-formulated NLP problem is solved by dynamic programming, which is known to be highly dependent on the initial guess to avoid getting stuck in local optima [30, 33]. Therefore, the selection of an adequate initial guess is critical, so a specific method for retrieving a well-structured guess towards the global optimum is described in the next section.

4.2 Initial guess

An adequate initial guess is required to find optimal solutions for the STL motion planner in a reasonable time and to prevent the solver from getting stuck looking for a feasible solution. The key idea to retrieve this initial guess is abstracting the original diverter installation problem to come up with a simpler optimization with fewer constraints. In particular, the initial guess considers mission requirements related with visiting all target regions, taking into account UAV payload capacities and refilling operations (φ_{tr}, φ_{cap} and φ_{rs}). It neglects obstacle avoidance and safety distance requirements (φ_{obs}, φ_{ws} and φ_{dis}) and the mission time intervals (t_N, t_{ins} and t_{rs}), since these latter constraints introduce the most complex nonlinearities and motion discontinuities in the problem. A graph-based representation, including connections between the target regions and the refilling stations, is used to formulate an MILP that models a type of VRP, whose solution assigns the target regions to the vehicles and provides a navigation sequence for each UAV. An Integer Linear Programming (ILP) formulation is not possible because the total distances covered by each UAV (real-valued variables) are considered in the optimization, in order to distribute them as equally as possible among the team members.

Figure 3 depicts an instance of the graph used, which is an undirected weighted multigraph described by the tuple $G = (\mathcal{V}, \mathcal{E}, \mathcal{W}, \mathcal{D}, \mathcal{C})$. The set of vertices is $\mathcal{V} = \mathcal{T} \cap \mathcal{R} \cap \mathcal{O}$, where $\mathcal{T}$ and $\mathcal{R}$ are the sets representing the locations of the target regions and the refilling stations, respectively, and $\mathcal{O}$ incorporates the set of depots where each UAV is located at time t_0, with $|\mathcal{T}| = \tau$, $|\mathcal{R}| = r$ and $|\mathcal{O}| = \delta$. The set of graph edges and their corresponding weights are given by $\mathcal{E}$ and $\mathcal{W}$, respectively; whereas, $\mathcal{D}$, with $|\mathcal{D}| = \delta$, represents the set of UAVs and $\mathcal{C}$ their corresponding maximum payload capacities. Concerning the connectivity of the graph, all vertices in $\mathcal{T}$ are fully connected to each other and to every vertex in the set $\mathcal{R} \cup \mathcal{O}$, each connection consisting of δ edges, one per UAV. More formally, let $e_{ij\|d} \in \mathcal{E}$ be the edge connecting the vertices i and j, with $\{i, j\} \in \mathcal{V}, i \neq j$, using UAV $d \in \mathcal{D}$, with $d = \{1, \ldots, \delta\}$; and $w_{ij\|d} \in \mathcal{W}$ the weight associated with $e_{ij\|d}$. Given the homogeneous dynamic constraints for UAVs $\bar{v}^{(j)}$ and $\bar{a}^{(j)}$, we model

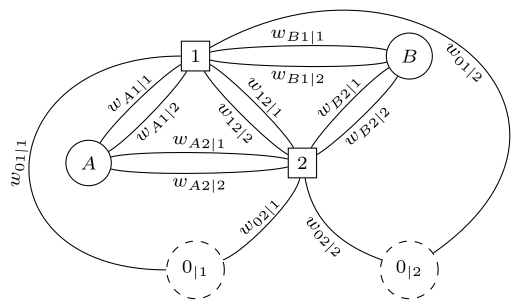

Figure 3: Instance of the graph G, assuming two target regions (square nodes), two refilling stations (round solid nodes) and two vehicles. Arcs and weights $w_{ij\|d}$ denote the UAVs' paths. Depots are depicted by round dashed nodes.

the edge weights using Euclidean distances, which implies $w_{ij\|d} = w_{ji\|d}$.

Given the graph G and the available UAVs with their capacities, the final objective is to find an optimal assignment that allocates to each UAV a sequence of target regions and refilling stations to visit, so that all diverters are installed, minimizing the mission time. Since the vehicles dynamic constraints are homogeneous ($\bar{v}^{(j)}$ and $\bar{a}^{(j)}$), as well as the flight times, minimizing the mission time could be equivalently translated into the problem of minimizing the distance covered by the multi-UAV team, but also evenly distributing the distances traveled by the vehicles, since the mission cannot be considered accomplished until the last UAV completes its sequence. Note that, including these travel distances implies the use of an MILP formulation instead of an ILP.

Associated with each edge $e_{ij\|d} \in \mathcal{E}$, an integer variable $z_{ij\|d} \in \mathbb{Z}_{\geq 0}$ can be defined such that $z_{ij\|d} = z_{ji\|d}$. This variable encodes the number of times that the corresponding edge is selected in the MILP solution. Thus, given a UAV $d \in \mathcal{D}$, $z_{ij\|d} \in \{0,1\}, \forall\{i,j\} \in \{\mathcal{T},\mathcal{O}\}$; and $z_{ij\|d} \in \{0,1,2\}$ if $i \in \mathcal{R}$ and $j \in \mathcal{T}$. The former ensures to never cover the edge between two target regions twice. In other words, starting from a depot without ever returning to it, and therefore depots are only start positions and not end positions. The latter allows for round trips between refilling stations and target regions in case there are no other diverters to be installed, i.e., $z_{ij\|d} = 2$. Whenever 0 appears in the subscript of the variable $z_{ij\|d}$, we refer to the i or j vertex as a depot, depending on the order. Furthermore, the real variables $\sigma_{rp} \in [0, \bar{\sigma}]$, with $\{r,p\} \in \mathcal{D}, r \neq p$, quantify the difference between the total distances covered by UAVs r and p, being $\bar{\sigma} \in \mathbb{R}_{\geq 0}$ this maximum acceptable difference. Using all these defined variables, the MILP problem can be formulated as follows:

$$\underset{z_{ij\|d},\sigma_{rp},y_{j\|d}}{\text{minimize}} \quad \sum_{\{i,j\}\in\mathcal{V},\, i\neq j,\, d\in\mathcal{D}} w_{ij\|d}\, z_{ij\|d} + \sum_{\{r,p\}\in\mathcal{D},\, r\neq p} \sigma_{rp} \tag{7a}$$

$$\text{s.t.} \quad \sum_{i\in\mathcal{V},\, i\neq j,\, d\in\mathcal{D}} z_{ij\|d} = 2,\ \forall j \in \mathcal{T}, \tag{7b}$$

$$\sum_{i\in\mathcal{V},\, i\neq j} z_{ij\|d} = 2y_{j\|d},\ \forall j \in \mathcal{T},\ \forall d \in \mathcal{D}, \tag{7c}$$

$$\sum_{i\in\mathcal{T}} z_{0i\|d} = 1,\ \forall d \in \mathcal{D}, \tag{7d}$$

$$\sum_{i\in\mathcal{T},\, j\notin\mathcal{T},\, d\in\mathcal{D}} z_{ij\|d} \geq 2h(\mathcal{T})\,, \tag{7e}$$

$$\sum_{\{i,j\}\in\mathcal{V},\, i\neq j} w_{ij\|r} z_{ij\|r} - w_{ij\|p} z_{ij\|p} - \sigma_{rp} \leq 0, \tag{7f}$$

$$\sum_{\{i,j\}\in\mathcal{V},\, i\neq j} w_{ij\|p} z_{ij\|p} - w_{ij\|r} z_{ij\|r} - \sigma_{rp} \leq 0, \tag{7g}$$

$$0 \leq \sigma_{rp} \leq \bar{\sigma},\ \forall\{r,p\} \in \mathcal{D},\ r \neq p,$$

where (7a) is the objective function, consisting of two terms that encode the total distance covered by the multi-UAV team, and a penalty for an uneven distance distribution between UAVs. Constraints (7b) and (7c) enforce that every target region is visited exactly once, being $y_{j\|d} \in \{0,1\}$ auxiliary integer variables that guarantee that, if $d \in \mathcal{D}$ UAV reaches the target $j \in \mathcal{T}$, the same UAV must also leave. (7d) ensures that every UAV starts the mission from its depot, but never returns. Constraints (7e) prevent the formation of tours exceeding the payload capacity of the UAVs or those which do not connect to a refilling station (i.e., the sub-tour elimination constraint [34, 35]). For that, $h(\mathcal{T})$ is a lower bound on the number of UAVs required to visit all target regions $\mathcal{T}$. In practice, it is common to define $h(\mathcal{T})$ as $\lceil \sum_{i\in\mathcal{T}} c_i/\mathcal{C} \rceil$. Due to the expensive computation of $h(\mathcal{T})$, these constraints are dynamically added as they are violated [35]. Finally, constraints (7f) and (7g) are used to bound the difference in distance covered by each pair of UAVs.

Once the MILP problem is solved, multirotor motion primitives [29, eq. (2)] are used to retrieve a dynamically feasible trajectory for each UAV, connecting target regions and refilling stations in its optimal assignment. The full description on how to compute these trajectories can be found in [36] and is not given here for the sake of brevity. In short, these motion primitives are computed fixing rest-to-rest motion between regions, i.e., zero velocity and acceleration in such regions, and imposing the minimum feasible time that allows the fulfillment of the desired maximum values of velocity $\bar{v}^{(j)}$ and acceleration $\bar{a}^{(j)}$ along the UAV's motion. Installation time intervals t_{ins} and refilling time intervals t_{rs} with the UAVs stopped in the corresponding regions are also considered for the trajectories.

4.3 Event-triggered replanner

The presented motion planner provides feasible trajectories for a multi-UAV team carrying out a mission for the installation of bird diverters. However, UAV failures (e.g., due to a battery or technical fault) may occur during the execution of the mission, causing vehicles to become out of service. In these cases, an alternative UAV should resume the pending tasks so that the mission is not interrupted, but is successfully accomplished. This is achieved using an online procedure for event-based replanning.

Every time an event happens, i.e., a UAV fails, a new plan is recomputed online using the motion planner in Sections 4.1 and 4.2. The trajectories of the UAVs working correctly are not computed again, as they can keep on with their original plans. The only new plan to be computed is the one corresponding to the *backup* UAV that is replacing the faulty one. Assuming that the failure event is detected at time $t_{\text{fail}} \in [t_0, t_N]$, a new trajectory for the backup UAV is generated within the time interval $[t_{\text{fail}} + t_{\text{rep}}, t_N]$, with t_{rep} being the maximum expected computation time for replanning[3]. Moreover, the motion planner uses the original trajectories of the non-faulty UAVs within the time interval $[t_{\text{fail}}+t_{\text{rep}}, t_N]$ for the safety distance requirement (φ_{dis}) as input constraints, as these do not need to be recomputed. Furthermore, only the pending (not visited) target regions previously assigned to the faulty UAV are considered in the replanning procedure. However, the order for visiting these target regions may change, as the backup UAV could start from a position or with a payload that makes that visit sequence suboptimal. Finally, it is worth mentioning that the computational effort for replanning is significantly lower than that for initial planning, as only a single UAV is considered with a reduced set of target regions (those not yet visited).

[3]The t_{rep} time was estimated by running several instances of the STL optimization problem and varying the number of target regions and their position, as well as the time instance t_{fail} when the fault occurs.

4.4 Energy-aware planner

This section presents an energy-aware extension of the motion planner in Section 4.1 for minimizing the energy consumed by the UAVs during the mission. The core idea is to determine the optimal cruising speed [37, Ch. 5], such that each UAV travels with minimal energy consumption and then tries to generate the vehicle's trajectories as close as possible to those nominal speeds. The computation of that optimal speed accounts for the aerodynamics of the multirotors to restrain the power demanded by the motors.

The electric power required by a multirotor decreases with increasing low forward speed. In contrast, this power increases dramatically at high speed due to parasitic losses [37, Ch. 5]. The combination of both effects leads to the existence of an optimal value for the forward speed that minimizes the energy consumption of the vehicle and extends its flight time. The authors in [37, Ch. 5] describe this energetically optimal forward speed $v^\star$ for multirotors as

$$v^\star = \sqrt{\frac{m}{2\varrho A}} \left(\frac{4\kappa A}{n_r f}\right)^{1/4}, \tag{8}$$

where $m \in \mathbb{R}$ is the mass of the vehicle, $n_r \in \mathbb{N}$ its number of rotors, $A \in \mathbb{R}$ the rotor disk area, $f \in \mathbb{R}$ the equivalent flat plate area of the fuselage, $\kappa \in \mathbb{R}$ an induced power correction factor, and $\varrho \in \mathbb{R}$ the air density.

The optimization problem (1) can be reformulated by including an energy term to favor solutions with a forward speed along the trajectory as close as possible to the ideal (in terms of energy consumption) value $v^\star$. Namely, we write

$$\begin{aligned} \underset{\mathbf{p}^{(j)}, \mathbf{v}^{(j)}, \mathbf{a}^{(j)}}{\text{maximize}} \quad & \tilde{\rho}_\varphi(\mathbf{p}^{(j)}, \mathbf{v}^{(j)}) - \eta \sum_k \left(1 - \frac{v_{\text{for}}(v_k)}{v^\star}\right)^2 \\ \text{s.t.} \quad & |v_k^{(j)}| \leq \bar{v}^{(j)}, |a_k^{(j)}| \leq \bar{a}^{(j)}, \\ & \mathbf{S}^{(j)}, \forall k = \{0, 1, \ldots, N-1\}, \end{aligned} \tag{9}$$

where $\eta \in [0,1]$ is a tunable parameter that weights the energy term in the objective function, and $v_{\text{for}}(v_k)$ is the multirotor forward speed for the time step t_k, defined along the x and y axes

$$v_{\text{for}}(v_k) = \sqrt{(v_k^{(1)})^2 + (v_k^{(2)})^2}. \tag{10}$$

Note that, as shown in [38], the energy expended by the multirotors for the ascent and descent maneuvers is constant, since it is performed at a constant speed. The same holds for the energy consumed during hovering operations. Therefore, with a good approximation, we can remove $v^{(3)}$ from (10), reducing the computational burden of the optimal problem (9).

It may happen that $v^\star$ is higher than the maximum feasible vehicle speed $\bar{v}^{(j)}$. In this case, the optimization problem (9) can be reformulated by replacing $v^\star$ with $\max(\bar{v}^{(1)}, \bar{v}^{(2)})$ as the feasible forward speed closest to $v^\star$ (8).

The new energy term is a quadratic error that measures how far the vehicle speed along the trajectory is from the one which minimizes energy consumption. Note that, the solutions of the energy-aware planner are still feasible trajectories complying with all mission requirements, although they trade off energy consumption with a possible decrease in robustness.

5 Experimental Results

To prove the validity and effectiveness of the proposed planning approach, we carried out numerical simulations in MATLAB. At this stage, the actual vehicle dynamics and the trajectory tracking controller were not modeled. Then we performed simulations on the Gazebo robotics simulator to verify the feasibility of the trajectories exploiting the benefits of software-in-the-loop simulations [39, 40]. Finally, field experiments in a mock-up scenario were performed to demonstrate the viability of the method for a real application. These experiments aim to demonstrate: (i) the compliance of the planned trajectories with the mission requirements; (ii) the need for the STL motion planner in order to meet the mission specifications, as the MILP formulation is not enough by itself; (iii) the capability to replan missions under UAV failures; (iv) a comparison of the solutions with and without the energy-aware feature; and (v) the feasibility of the method in real-world scenarios.

The optimization method was coded using MATLAB R2019b, with the MILP formulated using the CVX framework and the STL motion planner using the CasADi library and IPOPT as solver. All numerical simulations were run on a computer with an i7-8565U processor (1.80 GHz) and 32GB of RAM running on Ubuntu 20.04. Videos with the experimental results can be found at http://mrs.felk.cvut.cz/bird-diverter-ar.

Parameter	**Symbol**	**Value**
Payload capacity (UAV-1)	c_1	$2\,[-]$
Payload capacity (UAV-2)	c_2	$3\,[-]$
Payload capacity (UAV-3)	c_3	$4\,[-]$
Payload capacity (UAV-4)	c_4	$1\,[-]$
Safety mutual distance	Γ	$3\,[\mathrm{m}]$
Max. velocity	$\bar{v}^{(j)}$	$3.1\,[\mathrm{m/s}]$
Max. acceleration	$\bar{a}^{(j)}$	$3.1\,[\mathrm{m/s^2}]$
Optimal forward speed	$v^\star$	$2.5\,[\mathrm{m/s}]$
Time replanning	t_{rep}	$10\,[\mathrm{s}]$
Mission time	t_N	$155\,[\mathrm{s}]$
Installation time	t_{ins}	$5\,[\mathrm{s}]$
Refilling time	t_{rs}	$12\,[\mathrm{s}]$
Sampling period	T_s	$0.05\,[\mathrm{s}]$
Number of samples	N	$1360\,[-]$
Max. difference in distance	$\bar{\sigma}$	$10\,[\mathrm{m}]$
Scaling factor	λ	$10\,[-]$
Weight energy term	η	$1\,[-]$

Table 1: Parameter values for the optimization problem.

5.1 Bird diverters installation

The proposed planning strategy was tested for the bird diverter installation scenario described in Section 2. Specifically, as depicted in Figure 2, two UAVs were considered to operate in a mock-up scenario ($50\,\mathrm{m} \times 20\,\mathrm{m} \times 15\,\mathrm{m}$) with seven target regions and four refilling stations. Table 1 reports the parameters and their values used to run the optimization problem. It should be noted that the installation time t_{ins} and the refilling time t_{rs} were set using short symbolic times to avoid analyzing trajectories with excessively long waiting periods. The heading angles were adjusted and the vehicles aligned with the displacement direction if they were moving toward the target, while toward the cables during the installation operation. Once the UAV reaches a region, it is assumed that an onboard low-level controller will take care of the installation operation.

Figure 4 shows the planned trajectories along with power towers and cables, target regions, and refilling stations. The towers are $15\,\mathrm{m}$ in height and $40\,\mathrm{m}$ apart. The optimization problem took $14\,\mathrm{min}$ to solve and $37\,\mathrm{s}$ to find an initial guess solution. Figure 5 shows the compliance of the planned trajectories with mission requirements. As can be seen from the graph, the distance between vehicles is always greater than the

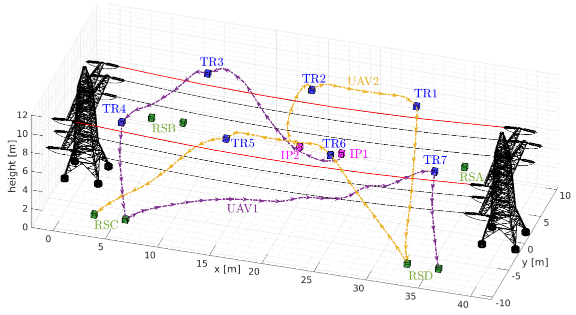
Figure 4: Bird diverter installation. Planned trajectories with two UAVs, seven target regions and four refilling stations. Arrows represent the UAVs' paths along the mission.

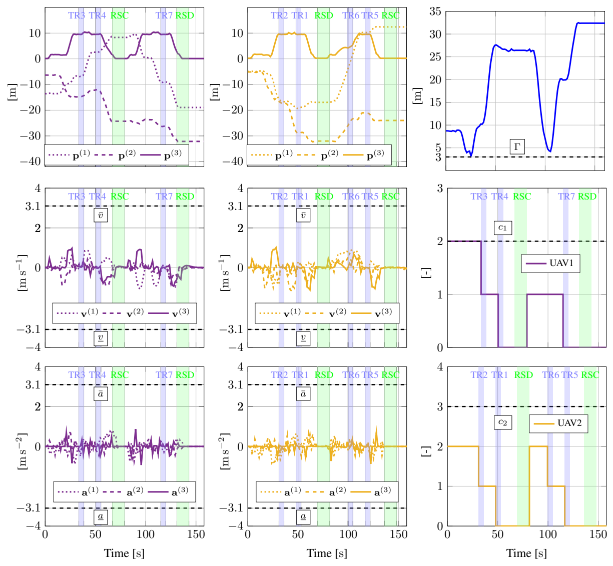
Figure 5: Position, linear velocity and acceleration, safety mutual distance, and payload capacity. From left to right: "UAV1" and "UAV2" data. The installation and refilling time windows are also reported using blue and green colors, respectively.

threshold value Γ, the vehicles' velocity and acceleration lie within the admissible bounds ($[\underline{v}^{(j)}, \bar{v}^{(j)}]$ and $[\underline{a}^{(j)}, \bar{a}^{(j)}]$), and the vehicles never visit a target region if they run out of diverters. Note that, for the sake of simplicity, the velocity and acceleration bounds are considered to be symmetric, i.e., $|\underline{v}^{(j)}| = |\bar{v}^{(j)}|$ and $|\underline{a}^{(j)}| = |\bar{a}^{(j)}|$. Finally, for comparison, Figure 6 reports the planned trajectories for a more complex setting, considering four UAVs and eleven target regions. In this case, the optimization problem took $22\,\mathrm{min}$ to solve, $57\,\mathrm{s}$ to find an initial guess solution.

5.2 Comparison with the initial guess solution

As described in Section 4, an MILP formulation is used to seed the STL optimization problem to generate feasible trajectories for the UAVs. Such a solution favors the convergence of the optimization problem towards solutions fulfilling all mission specifications. In fact, it could be the case where the solver easily gets stuck in local optima due to the NP-hard structure of the problem (1). However, the MILP solution, which can be computed more efficiently, is not enough by itself, as it does not take into account several nonlinear complexities of the problem, such as obstacle avoidance and safety distance requirements. Therefore, the final STL optimization works by refining the initial guess solution until the maximum robustness value is reached. In this regard, this section compares the initial solution obtained by solving the MILP (7) formulation with that retrieved by the STL optimization problem (1), in an attempt to understand how well (poorly) the specifications are met and whether it is worth applying this hierarchical solution to the problem. Figure 7 shows the dynamically feasible trajectories obtained using the multirotor motion primitives [29] and the sequences of waypoints assigned by the MILP solution to each UAV.

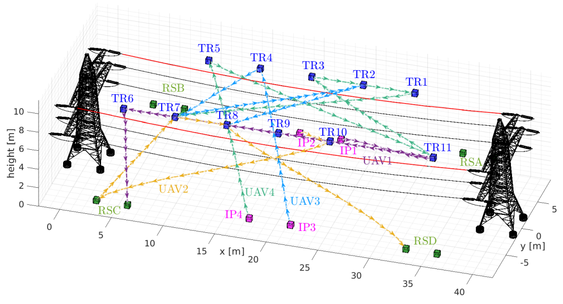
Figure 6: Bird diverter installation. Planned trajectories with four UAVs, eleven target regions and four refilling stations.

From a first glance, it is worth noting that the MILP formulation does not explicitly take time into account. This ends up in trajectories that could exceed the time bound t_N, resulting as impractical in real-world scenarios. This also has repercussions from a trajectory point of view, as the MILP approach

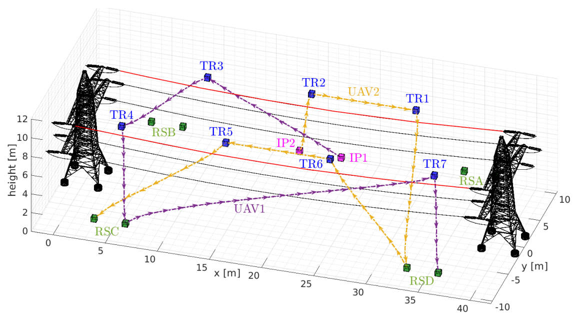

Figure 7: Bird diverter installation considering the trajectories obtained by solving just the MILP formulation, without applying the STL planner.

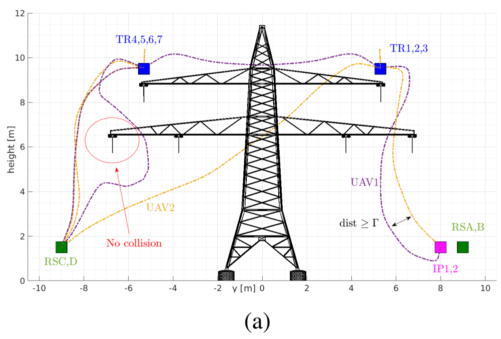

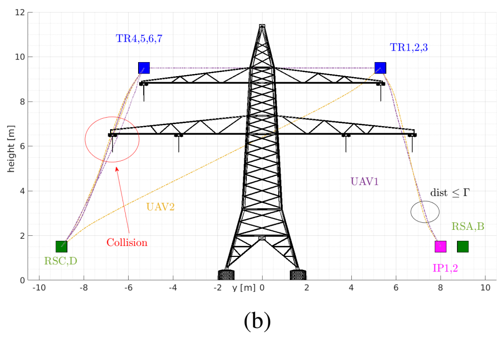

Figure 8: The trajectories obtained by using the whole STL (8a) and only the MILP (8b) optimization problems.

does not act on accelerations $\mathbf{a}^{(j)}$ to control the vehicles' motion (see [29, eq. (2)]), but rather on their position by setting the waypoint sequences that UAVs should visit to meet mission specifications. This implies spikes and corners that are difficult to follow in reality, possibly leading to sudden stresses on the actuators to respond to rather fast changes of direction. This results not only in possible errors in trajectory tracking, with the possibility of violating mission specifications and safety requirements (e.g., the UAVs could collide with power towers or cables), but also in high energy consumption that could harm the mission. Another important difference lies in the mutual safety distance constraint (φ_{dis}). While this constraint can be achieved in the STL optimization problem by regulating the vehicles' velocities and accelerations, and hence their positions, without affecting the optimal sequence of regions to visit, this does not apply to the MILP formulation, where vehicle dynamics are not taken into consideration to limit the computational burden. In actuality, increases in the values of Γ (3c) might require completely different optimal sequences (output of the MILP solver) for the final solution of the problem.

Figure 8 depicts the difference between the solutions obtained by solving only the MILP and the whole STL optimization problems. As can be seen in the figure, the STL formulation fine tunes the initial guess solution to achieve obstacle avoidance and safety distance requirements, along with the other mission specifications. In particular, it is evident how the trajectories are completely rearranged to reach higher robustness values $\tilde{\rho}_{\varphi}(\mathbf{x})$.

Lastly, it is worth mentioning that the differences between the STL and MILP solutions are not only based on the shape of the trajectories, but also on the sequence of targets to visit. Figure 9 shows a simple scenario where two UAVs (located at “IP1” and “IP2”), having the same dynamic constraints, are required to visit a set of target regions (“TR1”, “TR2”, “TR3” and “TR4”) within the time interval $[0, t_N]$, while remaining in the workspace area (φ_{ws}), avoiding obstacles (φ_{obs}), and maintaining a safe distance with each other (φ_{dis}). As can be seen, the MILP initial guess (Figure 9b) proposes an assignment of target regions that balances the workload between UAVs and minimizes the distance traveled, although crossing the obstacle as obstacle avoidance is not taken into account in problem formulation. Conversely, despite this initial guess solution, the whole STL planner (Figure 9a) rearranges the target assignment to comply with all mission specifications. Such a simple scenario shows the independence of the final STL optimization from the MILP initial guess solution, which brings additional flexibility to the hierarchical planner. However, as the complexity of the problem increases, having an initial guess away from the entire problem solution may result in the STL optimizer getting stuck in a local optima.

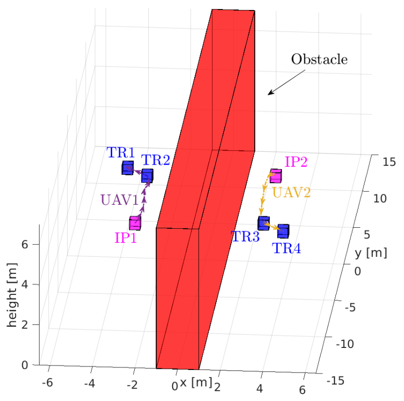

(a)

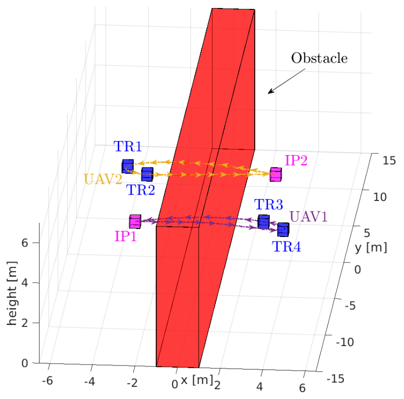

(b)

Figure 9: Simple scenario showing the independence of the final STL solution (9a) from the MILP initial guess (9b).

5.3 Energy-aware and replanning strategy

This section aims to show the capability of the *energy-aware* and *event-triggered replanner*, described in Sections 4.4 and 4.3, to reduce the energy consumed by the UAVs during mission execution and to ensure mission continuity in the event of a UAV failure, respectively. The results of the numerical simulations carried out in MATLAB are depicted in Figures 10 and 12. Regarding the energy-aware planner, the trajectories considering the forward speed term $v^{\star}$ (see Figure 10) are longer and marked by sudden changes of direction compared to the case when no energy requirement is enforced (see Figures 4 and 6). This fact is motivated by the need of the UAVs to perform the installation of diverters approaching the energetically optimal forward speed $v^{\star}$, while also satisfying the mission specifications φ (see eq. (2)). Therefore, the leeway of the optimization problem (9) in the velocity of the vehicle is less than in the case of the standard planner (1), where the velocity values can be adjusted within a much wider range to maximize the robustness score. Figure 11 shows the comparison between forward speed v_{for} and robustness values $\tilde{\rho}_{\varphi}(\mathbf{x})$ for the standard and energy-aware planners. As can be seen in the plot, increases in velocity come at the expense of a slight reduction in robustness values.

To showcase the event-triggered replanner, we considered the case with a pair of UAVs performing the installation of bird diverters. In particular, the scenario where the two UAVs start the mission

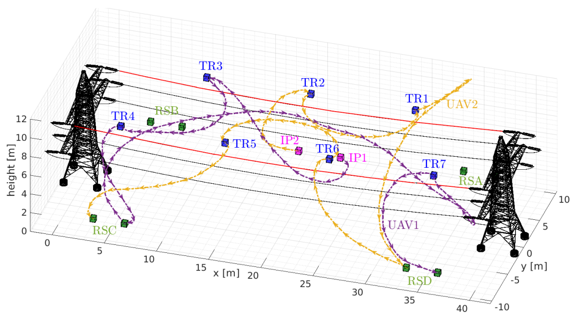

Figure 10: Bird diverter installation when considering the solution retrieved by the energy-aware planner.

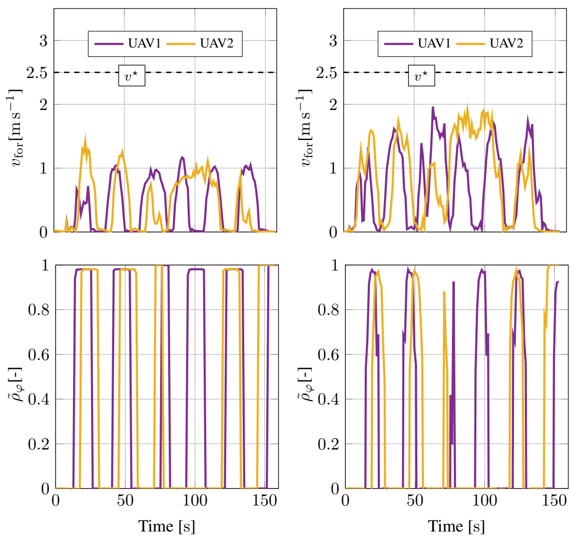

Figure 11: From left to right: a comparison between the forward speed $v_{\text{for}}(v_k)$ and the normalized robustness values $\tilde{\rho}_{\varphi}(\mathbf{x})$ when considering the standard and the energy-aware planner.

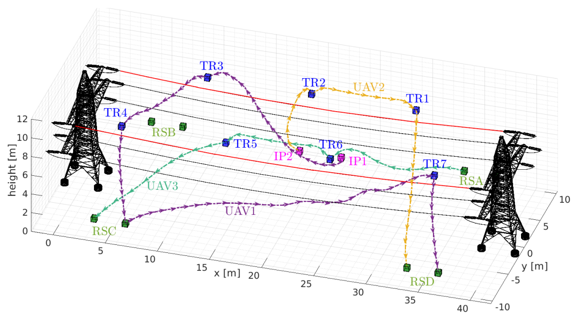

Figure 12: Bird diverter installation in case of “UAV2” failure running in the “RSD” refilling station. In green, the path of the backup vehicle, i.e., “UAV3”.

by tracking the trajectories shown in Figure 4. We then simulate a failure event that occurs when one of the UAVs, specifically “UAV2” (see Figure 12), visits a refilling station to bring on board new diverters. This event triggers the execution of the optimization problem (1), and therefore the resolution of the related MILP (7) for the backup vehicle (i.e., “UAV3”) at disposal at one of the refill stations (“RSA” for the considered scenario), by considering the pending regions of “UAV2” (those not yet visited) and the trajectory of the non-faulty UAV (i.e., “UAV1”). The resulting trajectories are shown in Figure 12. For this particular scenario, the same order is maintained for visiting the target regions while slight variations in the trajectory connecting “TR5” and “RSC” can be observed. This trajectory change is driven by the optimization problem to meet safety and obstacle avoidance requirements. The optimization took 2 s to solve the entire problem and a few tenths of a second for the MILP. The failure was detected at $t_{\text{fail}} = 9\,\text{s}$, considering a maximum expected computation time of $t_{\text{rep}} = 10\,\text{s}$.

5.4 Field experiments

To evaluate and prove the applicability of the proposed motion planning approach in real-world applications, experiments with DJI F450 quadrotors [41] were performed in a mock-up scenario. The scenario depicted in Figure 4 with two UAVs was considered. For ease of experimentation and taking into account the complexity of flying in such a safety-critical scenario as that of the power line, we simulated both power towers and cables along with the location of the refilling stations. Therefore, the UAVs flew in a large workspace area

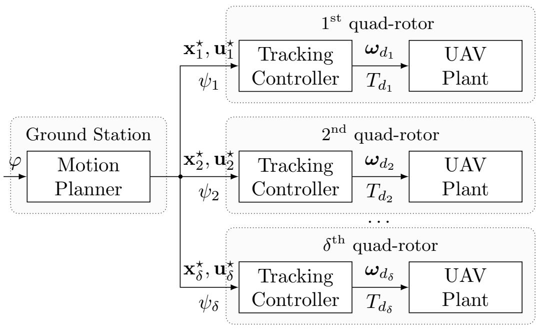
1st quad-rotor
2nd quad-rotor
δth quad-rotor
Ground Station
Motion Planner
Tracking Controller
UAV Plant
φ
$\mathbf{x}_1^\star, \mathbf{u}_1^\star$
ψ_1
$\boldsymbol{\omega}_{d_1}$
T_{d_1}
$\mathbf{x}_2^\star, \mathbf{u}_2^\star$
ψ_2
$\boldsymbol{\omega}_{d_2}$
T_{d_2}
$\mathbf{x}_\delta^\star, \mathbf{u}_\delta^\star$
ψ_δ
$\boldsymbol{\omega}_{d_\delta}$
T_{d_δ}

Figure 13: The system architecture. The *STL Motion Planner* running on a ground station supplies the trajectories $(\mathbf{x}_1^\star, \mathbf{u}_1^\star, \dots, \mathbf{x}_\delta^\star, \mathbf{u}_\delta^\star,)$ and the heading angles $(\psi_1, \dots, \psi_\delta)$ to the multirotors' *Tracking Controller*, which outputs the thrust $(T_{d_1}, \dots, T_{d_\delta})$ and angular velocities $(\boldsymbol{\omega}_{d_1}, \dots, \boldsymbol{\omega}_{d_\delta})$ for the *UAV Plant* [29, 39, 41].

tracking trajectories designed in MATLAB and validated in Gazebo, where the presence of those objects was taken into account. Videos with simulated and experimental results can be found in http://mrs.felk.cvut.cz/bird-diverter-ar.

The system architecture is reported in Figure 13. The STL motion planner solves the optimization problem (1) for supplying the trajectories $(\mathbf{x}^\star, \mathbf{u}^\star)$ and the heading angles ψ to the multirotors. The trajectory generation is run one-shot, i.e., once at time t_0. The result is used as reference by the UAV trajectory tracking controller [39]. As for the hardware, the UAVs were equipped with an Intel NUC computer on board (an i7-8559U processor with 16GB of RAM) and the Pixhawk flight controller. The software stack was built on the Noetic Ninjemys release of the Robot Operating System (ROS) running on Ubuntu 20.04. Further details are available in [41].

Real flights were able to not only verify the fulfillment of the installation mission expressed by the STL formula (2), but also the compliance with physical constraints and safety requirements ($\bar{v}$, $\bar{a}$, and Γ), as well as the vehicles' payload capacity $c_\bullet$ (see Table 1). Figure 14 depicts some snapshots of the experiment. To provide a sense of how close (distance) the UAVs were with respect to the mechanical infrastructure (cables and towers) and refilling locations, these were virtualized by means of a ROS package projecting within the UAVs' camera frames the 3D mesh files used in MATLAB and Gazebo to represent the scenario.

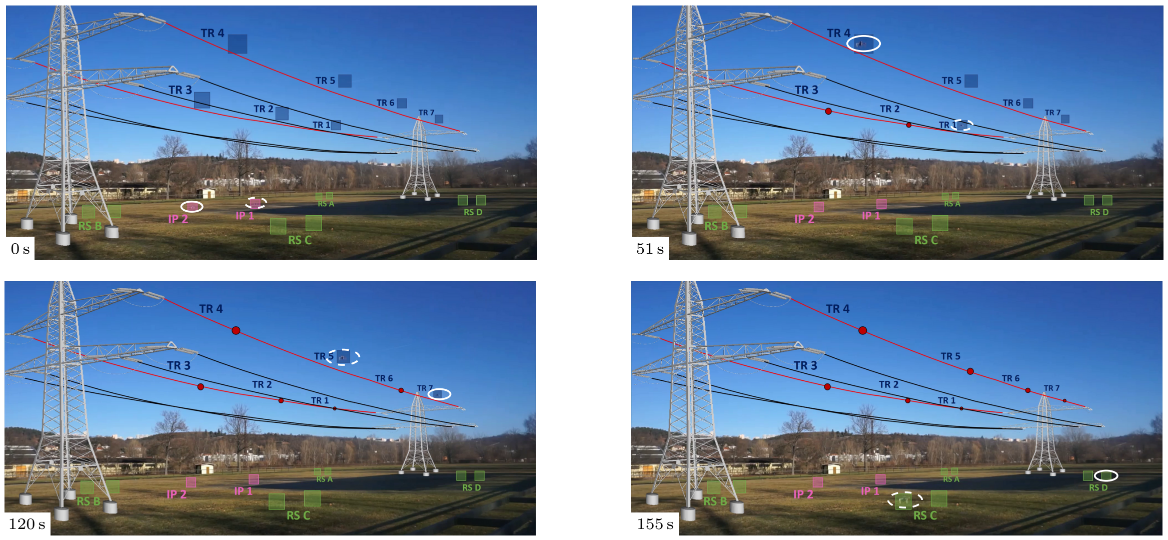

Figure 14: Snapshots of the field experiment. The system evolution at different time instants t_k is reported. Solid and dashed white lines are used to indicate the position of "UAV1" and "UAV2", respectively. Power towers and cables are virtualized in the frames to better clarify the scenario. Targets regions, refilling stations, and UAVs' initial positions are depicted using blue, green, and magenta squares, respectively. Red spheres show the already visited regions at each snapshot.

6 Conclusions

This paper has presented a motion planning framework for encoding bird diverter installation missions for a team of multirotors endowed with payload capacity limitations and dynamic constraints. The proposed method uses STL specifications to generate dynamically feasible trajectories that comply with mission specifications, including safety and mission time requirements. The work extended a previous authors' motion planner [29] by proposing a way to tackle the nonlinear non-convex nature of the optimization problem towards the use of an MILP approach. Such an approach runs over a simplification of the mission specifications to provide a feasible initial guess solution for the STL framework to favor the convergence of the algorithm. Furthermore, an event-triggered replanner and an energy-aware planner have been proposed to reply to UAV failures that may occur during mission execution and to improve multirotor energy savings in the installation process, respectively. Numerical simulations in MATLAB and Gazebo, in addition to field experiments, demonstrated the validity of the proposed approach, proving its applicability in real-world applications through the use of a mock-up scenario.

Our numerical analysis showed that, by itself, the simplified MILP solver is not sufficient for the purpose of the application. It serves as an initial guess to ease the convergence of the complete STL planner, but this may end up with quite different solutions with respect to the initial guess. Thanks to our hierarchical approach including both solvers, we are able to tackle in an integrated optimization problem a richer set of mission specifications and requirements than others in the state-of-the-art, although this comes at the expense of an increase in the computational complexity. Future work includes investigating methods to relax this computational load and improve scalability by accounting for decentralized feedback control laws based on time-varying control barrier functions. In addition, we plan to investigate the use of conflicting temporal logic specifications and other types of temporal logic languages to apply the framework for dynamically changing environments.

Acknowledgments. This work was funded by the European Union's Horizon 2020 research and innovation programme AERIAL-CORE under grant agreement no. 871479. The authors would like to thank Daniel Smrcka, Jan Bednar, Jiri Horyna, Tomas Baca, Martin Saska and the MRS group in Prague for their help with the field experiments. The authors would like to thank Jesus Capitan for his advice and valuable feedback to the development of the technical part.

References

[1] Hunting, K.: A Roadmap for PIER Research on Avian Collisions with Power Lines in California. Commission Staff Report. California Energy Commission, https://tinyurl.com/3v6yrehm (2002)

[2] Ferrer, M., Morandini, V., Baumbusch, R., Muriel, R., De Lucas, M., Calabuig, C.: Efficacy of different types of "bird flight diverter" in reducing bird mortality due to collision with transmission power lines. Global Ecology and Conservation **23**, 01130 (2020). https://doi.org/10.1016/j.gecco.2020.e01130

[3] Suarez, A., Romero, H., Salmoral, R., Acosta, J.A., Zambrano, J., Ollero, A.: Experimental Evaluation of Aerial Manipulation Robot for the Installation of Clip Type Bird Diverters: Outdoor Flight Tests. In: Aerial Robotic Systems Physically Interacting with the Environment, pp. 1–7 (2021). https://doi.org/10.1109/AIRPHARO52252.2021.9571029

[4] Rodriguez-Castano, A., Nekoo, S.R., Romero, H., Salmoral, R., Acosta, J.A., Ollero, A.: Installation of Clip-Type Bird Flight Diverters on High-Voltage Power Lines with Aerial Manipulation Robot: Prototype and Testbed Experimentation. Applied Sciences **11**(16) (2021). https://doi.org/10.3390/app11167427

[5] Suarez, A., Salmoral, R., Zarco-Periñan, P.J., Ollero, A.: Experimental Evaluation of Aerial Manipulation Robot in Contact With 15 kV Power Line: Shielded and Long Reach Configurations. IEEE Access **9**, 94573–94585 (2021). https://doi.org/10.1109/ACCESS.2021.3093856

[6] Armengol, I., Suarez, A., Heredia, G., Ollero, A.: Design, Integration and Testing of Compliant Gripper for the Installation of Helical Bird Diverters on Power Lines. In: Aerial Robotic Systems Physically Interacting with the Environment, pp. 1–8 (2021). https://doi.org/10.1109/AIRPHARO52252.2021.9571044

[7] Afifi, A., van Holland, M., Franchi, A.: Toward Physical Human-Robot Interaction Control with Aerial Manipulators: Compliance, Redundancy Resolution, and Input Limits. In: International Conference on Robotics and Automation, pp. 4855–4861 (2022). https://doi.org/10.1109/ICRA46639.2022.9812451

[8] Pola, G., Di Benedetto, M.D.: Control of Cyber-Physical-Systems with logic specifications: A formal methods approach. Annual Reviews in Control **47**, 178–192 (2019). https://doi.org/10.1016/j.arcontrol.2019.03.010

[9] Maler, O., Nickovic, D.: Monitoring temporal properties of continuous signals. In: Formal Techniques, Modelling and Analysis of Timed and Fault-Tolerant Systems, pp. 152–166. Springer, Berlin, Heidelberg (2004). https://doi.org/10.1007/978-3-540-30206-3_12

[10] Karaman, S., Frazzoli, E.: Sampling-based algorithms for optimal motion planning. The International Journal of Robotics Research **30**(7), 846–894 (2011). https://doi.org/10.1177/0278364911406761

[11] Hauser, K., Zhou, Y.: Asymptotically Optimal Planning by Feasible Kinodynamic Planning in a State-Cost Space. IEEE Transactions on Robotics **32**(6), 1431–1443 (2016). https://doi.org/10.1109/TRO.2016.2602363

[12] Webb, D.J., van den Berg, J.: Kinodynamic RRT*: Asymptotically optimal motion planning for robots with linear dynamics. In: IEEE International Conference on Robotics and Automation, pp. 5054–5061 (2013). https://doi.org/10.1109/ICRA.2013.6631299

[13] Ryll, M., Ware, J., Carter, J., Roy, N.: Efficient trajectory planning for high speed flight in unknown environments. In: International Conference on Robotics and Automation, pp. 732–738 (2019). https://doi.org/10.1109/ICRA.2019.8793930

[14] Chen, G., Sun, D., Dong, W., Sheng, X., Zhu, X., Ding, H.: Computationally Efficient Trajectory Planning for High Speed Obstacle Avoidance of a Quadrotor With Active Sensing. IEEE Robotics and Automation Letters **6**(2), 3365–3372 (2021). https://doi.org/10.1109/LRA.2021.

3062332

[15] Nekovář, F., Faigl, J., Saska, M.: Multi-Tour Set Traveling Salesman Problem in Planning Power Transmission Line Inspection. IEEE Robotics and Automation Letters **6**(4), 6196–6203 (2021). https://doi.org/10.1109/LRA.2021.3091695

[16] Coutinho, W.P., Battarra, M., Fliege, J.: The unmanned aerial vehicle routing and trajectory optimisation problem, a taxonomic review. Computers & Industrial Engineering **120**, 116–128 (2018). https://doi.org/10.1016/j.cie.2018.04.037

[17] Penicka, R., Faigl, J., Saska, M.: Physical Orienteering Problem for Unmanned Aerial Vehicle Data Collection Planning in Environments With Obstacles. IEEE Robotics and Automation Letters **4**(3), 3005–3012 (2019). https://doi.org/10.1109/LRA.2019.2923949

[18] Penicka, R., Scaramuzza, D.: Minimum-Time Quadrotor Waypoint Flight in Cluttered Environments. IEEE Robotics and Automation Letters **7**(2), 5719–5726 (2022). https://doi.org/10.1109/LRA.2022.3154013

[19] Penicka, R., Song, Y., Kaufmann, E., Scaramuzza, D.: Learning Minimum-Time Flight in Cluttered Environments. IEEE Robotics and Automation Letters **7**(3), 7209–7216 (2022). https://doi.org/10.1109/LRA.2022.3181755

[20] Nguyen, H., Kamel, M., Alexis, K., Siegwart, R.: Model Predictive Control for Micro Aerial Vehicles: A Survey. In: European Control Conference, pp. 1556–1563 (2021). https://doi.org/10.23919/ECC54610.2021.9654841

[21] Robinson, D.R., Mar, R.T., Estabridis, K., Hewer, G.: An Efficient Algorithm for Optimal Trajectory Generation for Heterogeneous Multi-Agent Systems in Non-Convex Environments. IEEE Robotics and Automation Letters **3**(2), 1215–1222 (2018). https://doi.org/10.1109/LRA.2018.2794582

[22] Luis, C.E., Vukosavljev, M., Schoellig, A.P.: Online trajectory generation with distributed model predictive control for multi-robot motion planning. IEEE Robotics and Automation Letters **5**(2), 604–611 (2020). https://doi.org/10.1109/LRA.2020.2964159

[23] Alcántara, A., Capitán, J., Cunha, R., Ollero, A.: Optimal trajectory planning for cinematography with multiple unmanned aerial vehicles. Robotics and Autonomous Systems **140**, 103778 (2021). https://doi.org/10.1016/j.robot.2021.103778

[24] Chen, Y., Ding, X.C., Stefanescu, A., Belta, C.: Formal Approach to the Deployment of Distributed Robotic Teams. IEEE Transactions on Robotics **28**(1), 158–171 (2012). https://doi.org/10.1109/TRO.2011.2163434

[25] Lindemann, L., Dimarogonas, D.V.: Barrier Function Based Collaborative Control of Multiple Robots Under Signal Temporal Logic Tasks. IEEE Transactions on Control of Network Systems **7**(4), 1916–1928 (2020). https://doi.org/10.1109/TCNS.2020.3014602

[26] Gilpin, Y., Kurtz, V., Lin, H.: A Smooth Robustness Measure of Signal Temporal Logic for Symbolic Control. IEEE Control Systems Letters **5**(1), 241–246 (2021). https://doi.org/10.1109/LCSYS.2020.3001875

[27] Leahy, K., Serlin, Z., Vasile, C.-I., Schoer, A., Jones, A.M., Tron, R., Belta, C.: Scalable and Robust Algorithms for Task-Based Coordination From High-Level Specifications (ScRATCHeS). IEEE Transactions on Robotics **38**(4), 2516–2535 (2022). https://doi.org/10.1109/TRO.2021.3130794

[28] Muniraj, D., Vamvoudakis, K.G., Farhood, M.: Enforcing Signal Temporal Logic Specifications in Multi-Agent Adversarial Environments: A Deep Q-Learning Approach. In: IEEE Conference on Decision and Control, pp. 4141–4146 (2018). https://doi.org/10.1109/CDC.2018.8618746

[29] Silano, G., Baca, T., Penicka, R., Liuzza, D., Saska, M.: Power Line Inspection Tasks With Multi-Aerial Robot Systems Via Signal Temporal Logic Specifications. IEEE Robotics and Automation Letters **6**(2), 4169–4176 (2021). https://doi.org/10.1109/LRA.2021.3068114

[30] Bertsekas, D.: Dynamic Programming and Optimal Control, Athena Scientific (2012)

[31] Donzé, A., Maler, O.: Robust satisfaction of temporal logic over real-valued signals. In: International Conference on Formal Modeling and Analysis of Timed Systems, pp. 92–106 (2010). https://doi.org/10.1007/978-3-642-15297-9_9. Springer

[32] Fainekos, G.E., Pappas, G.J.: Robustness of temporal logic specifications for continuous-time signals. Theoretical Computer Science **410**(42), 4262–4291 (2009). https://doi.org/10.1016/j.tcs.2009.06.021

[33] Cai, Y., Judd, K.L., Lontzek, T.S., Michelangeli, V., Su, C.-L.: A Nonlinear Programming Method For Dynamic Programming. Macroeconomic Dynamics **21**(2), 336–361 (2017). https://doi.org/10.1017/S1365100515000528

[34] Miller, C., Tucker, A., Zemlin, R.A.: Integer programming formulation of traveling salesman problems. Journal of the Association for Computing Machinery **7**, 326–329 (1960). https://doi.org/10.1145/321043.321046

[35] Laporte, G.: What you should know about the vehicle routing problem. Naval Research Logistics **54**(8), 811–819 (2007). https://doi.org/10.1002/nav.20261

[36] Mueller, M.W., Hehn, M., D'Andrea, R.: A Computationally Efficient Motion Primitive for Quadrocopter Trajectory Generation. IEEE Transactions on Robotics **31**(6), 1294–1310 (2015). https://doi.org/10.1109/TRO.2015.2479878

[37] Leishman, G.J.: Principles of Helicopter Aerodynamics, Cambridge University Press (2006)

[38] Carmelo, D., Giorgio, B.: Coverage Path Planning for UAVs Photogrammetry with Energy and Resolution Constraints. Journal of Intelligent & Robotic Systems **83**, 445–462 (2016). https://doi.org/10.1007/s10846-016-0348-x

[39] Baca, T., Petrlik, M., Vrba, M., Spurny, V., Penicka, R., Hert, D., Saska, M.: The MRS UAV System: Pushing the Frontiers of Reproducible Research, Real-world Deployment, and Education with Autonomous Unmanned Aerial Vehicles. Journal of Intelligent & Robotic Systems **102**(26), 1–28 (2021). https://doi.org/10.1007/s10846-021-01383-5

[40] Silano, G., Oppido, P., Iannelli, L.: Software-in-the-loop simulation for improving flight control system design: a quadrotor case study. In: IEEE International Conference on Systems, Man and Cybernetics (SMC), pp. 466–471 (2019). https://doi.org/10.1109/SMC.2019.8914154

[41] Hert, D., Baca, T., Petracek, P., Kratky, V., Spurny, V., Petrilik, M., Matous, V., Zaitlik, D., Stoudek, P., Walter, V., Stepan, P., Horyna, J., Ptrizl, V., Silano, G., Bonilla Licea, D., Stibinger, P., Penicka, R., Nascimento, T., Saska, M.: MRS Modular UAV Hardware Platforms for Supporting Research in Real-World Outdoor and Indoor Environments. In: International Conference on Unmanned Aircraft Systems, pp. 1264–1273 (2022). https://doi.org/10.1109/ICUAS54217.2022.9836083